A Study on-resistance characteristics and turbulent structure properties of hyper◻concentrated sediment-laden flow

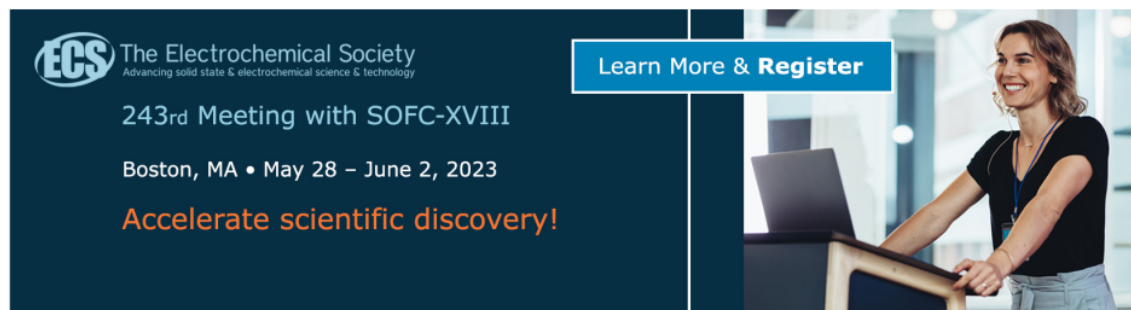*by* Liany Hendratta

PAPER · OPEN ACCESS

A Study on-resistance characteristics and turbulent structure properties of hyper-concentrated sediment-laden flow

To cite this article: L A Hendratta et al 2020 IOP Conf. Ser.: Earth Environ. Sci. **419** 012111

View the article online for updates and enhancements.

You may also like

A Study on-resistance characteristics and turbulent structure properties of hyper-concentrated sediment-laden flow

L A Hendratta[1], Sukarno[1] and T Ohmoto[2]

[1]Civil Engineering Department, Sam Ratulangi University, Manado, Indonesia
[2]Civil and Environmental Engineering Department, Kumamoto University, Kumamoto, Japan

Email: unsrat.ac.id

Abstract. Sediment laden flows of high density occur in most natural environments in the world. A certain amount of particles in hyper-concentrated sediment-laden flow plays an important role and has a great effect on the behavior of the flow. Significant erosion and siltation associated with hyper-concentrated floods give rise to many problems. Mudflows that contain large concentrations of clay particles suspended in water are considered to have non-Newtonian hydrodynamic properties but remain largely unknown. In this experimental study, the flow field over a square ribs roughness in an open channel was investigated in detail through comparison with clear water flow by using sodium polyacrylate (PSA) solutions that have viscosity characteristics similar to those of hyper-concentrated sediment-laden flow and applying PIV (Particle Image Velocimetry) measurement system to current meters. The experimental results stressed that the total resistance coefficient for the highly viscous PSA solution reached a maximum of 1.76 times the total resistance coefficient in clear water due to the shear-thinning effect of a non-Newtonian fluid.

1. Introduction

Hyper-concentrated sediment-laden flows contain a large volume of fine-grained sediment. They are observed under various conditions, such as the mudflow in rivers near the Tondano River basin, and tidal flows that contain the soil of tidal lands in the Tondano River estuary. In the aftermath of the Tondano River flood disaster in Manado, Indonesia, the volumetric concentration of sediment reached about 9.8%. The dynamic characteristics of hyper-concentrated sediment-laden flows are notably different than those of clear water. In addition to sediment concentration, the particle size, shape, distribution, and mineral content affect the properties of hyper-concentrated sediment-laden flows. The increased viscosity and density in sediment-laden flow would lead to changes in turbulence intensity, particle distribution, resistance characteristics, and sediment transport; however, it is not yet clear how those changes affect the flow dynamics of hyper-concentrated sediment-laden flows.

There is no consensus definition of hyper-concentrated sediment-laden flows. Flows with less than 20% volumetric concentration of sediment, which had minimal influence on density and viscosity identified as standard flows; flows with more than 20% volumetric concentration of sediment displayed more apparent influences on density and viscosity; non-Newtonian fluid characteristics were observed in sediment-laden flows with less than 5% volumetric concentration of clay and silt [1].

Several theoretical approaches can be used to study sediment-laden flows. The research took advantage of a Bingham fluid model while other explored functional relationships among yield stress,

viscosity coefficient, particle concentration, and particle size distribution using the pseudoplastic fluid model with yield stress [2, 3]. The study evaluated the bonding strength between each particle using the concept of an electric double layer with the Bingham fluid model and developed equations for yield stress and viscosity coefficient based on cutting energy associated with shearing [4]. However, these studies did not clarify the mechanism and effect of flow structure in non-Newtonian fluid or resistance law. The experiments conducted used small linear macromolecules in a closed conduit as a model for sediment-laden flows, and identified a notable decrease in the resistance characteristics compared to that of the solution without macromolecules; this was widely known as Tom's effect [5]. Similar effects have been observed in experimental flows containing a surfactant, pulp fiber, and fine bubbles. A closed-conduit experiment on flows that contained a surfactant and linear macromolecules reported a maximum decrease in flow resistance of 70% [6].

The present study investigated the effect of hyper-concentrated sediment on resistance and flow mechanism in an open-channel flow with two-dimensional square ribs. To determine the flow mechanism in detail, a sodium polyacrylate (PSA) solution that has viscosity characteristics similar to those of the hyper-concentrated kaolin sediment-laden flows was used. The flow velocities were measured by using particle image velocimetry (PIV) measurement system and compared the flow field in the PSA solution to that in clear water.

2. Methodology of the study

2.1 Experimental apparatus and method

In the experiment, the kaolin suspensions and PSA were made to flow in a circulating variable-slope flume measuring 10 m in length, 0.4 m in width and 0.2 m in height. The bottom and side of the flume were composed of acrylic resin that enabled laser light transmission and photography. The coordinate system on the right hand was used, and defined the x-, y-, and z-axes as the streamwise direction, the transverse direction, and the upward vertical direction, respectively. We defined the corresponding mean-flow velocity as U,V,W, and the various components as u^1, v^1, w^1. Figure 1 presents the details of the coordinate system.

(1) Double-pulsed LASER Illumination System
(2) Laser sheet
(3) YAG－Laser Main unit
(4) CCD- Camera Kodak Megaplus (ES1.0)
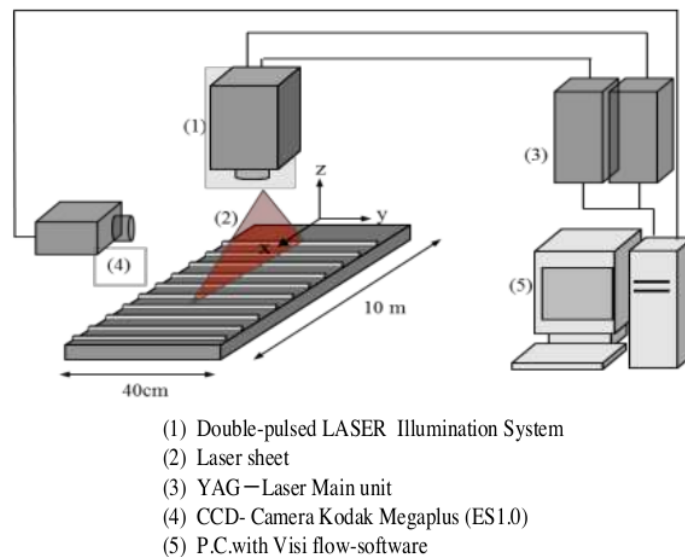(5) P.C.with Visi flow-software

Figure 1. Particle image velocimetry (PIV) measurement system.

Figure 2 illustrates the longitudinal arrangement for roughness. X_{RE} in the figure represents the flow distance from the rear edge. The ribs were made of stainless steel with a section of a square k=a=10 mm on aside. Sections of a rectangle k=5 mm and a=10 mm on sides were selected as the roughness material. The bed was set in a location 2 m from the upper reach of the channel at a length of 6 m in the flow direction.
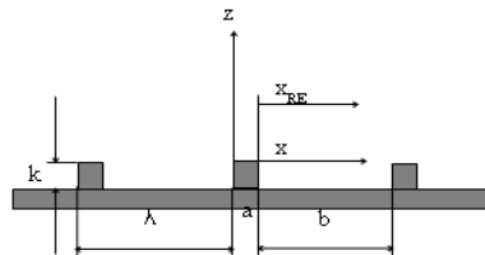

Figure 2. Channel bed configuration.

Table 1 presents the experimental conditions for examining the effect of sediment concentration on flow resistance. In the present experiment, we manipulated the sediment volumetric concentration and the concentration of sodium polyacrylate solution (Cw=0–800 mg/l) at intervals in the longitudinal direction λ/k=8 for k=5 mm and λ/k=10 for k=10 mm, respectively. Previous work indicates that these values of λ/k enable the drag coefficient to reach the maximum value in the clear water case [7]. The prescribed flow rate was adjusted by the weir at the downstream end to form the uniform flow field. The normal depth was measured at the uniform flow field with a gage point. The interval for the region of roughness was set at 6 m. The uniform flow field was identified in section 3–4 m in the center of the flume due to the consistency it demonstrated in the depth.

The sodium polyacrylate solutions, which mimicked hyper-concentrated sediment-laden flow at weight concentration levels of C_w=300–800 mg/l, corresponded to C_v =6% and 10% in sediment volumetric concentration for kaolin if calculated from the approximately similar resistance coefficient and viscosity coefficient. The advantages of using PSA solutions included the following: (1) it correctly reproduced hyper-concentrated sediment-laden flows under certain viscosity characteristics, and (2) the colorless and transparent nature of the solutions enabled PIV measurements to be performed.

In this experiment, flow resistance was calculated by measuring the water depth of a uniform flow field with point gauges. Also, for the purpose of checking on the uniformity distribution of kaolin suspension concentration, samples were taken at four points located in the region from the bed surface to the water surface

To measure the flow velocity, we modified the image-processing technique typically used for a contactless object using PIV. Figure 1 shows the details of the measurement system. The location of measurement was in the equivalent field, 4 m downstream from the tip of the rough surface. We used an air-cooled infrared pulsed laser as a light source for PIV. The optical sheet was adjusted to 1 mm in thickness with a pulse interval of 1000 μs. The light was transmitted vertically downward from the upper flume to the base. A visualization image captured through synchronization of the laser and the CCD camera was recorded on the hard disk of the computer as a monochrome video of 100 fps (frame per second) with an image resolution of 960×1018 pixels. These data were processed by PIV. A lens with a focal length of 50 mm was used. The smallest dimension for one pixel was 0.06 mm. The sampling frequency of the velocity measurement was 100 Hz. At one measurement site, 2000 samples of image data were collected. As a tracer, an 80 μm nylon particle with a specific gravity of 1.02 was thoroughly stirred with an alcohol solution and injected into the water. The experimental conditions for flow velocity are shown in table 2.

2.2 Experimental conditions

Table 1. Experimental conditions for flow resistance.

Case		Concentration	Discharge (l/s)	Channel slope (I_o)
Kaolin	k= 5mm	Cv = 0 ~ 12 %		
Suspension	k=10mm		4	1/500
PSA	k= 5mm	Cw= 0 ~ 800 mg/l		
solution	k=10mm			

Table 2. Experimental conditions for flow velocity.

		Case 1	Case 2	Case 3
PSA concentration	Cw (mg/l)	0	300	800
Discharge	Q (l/s)	4.0	4.0	4.0
Flow depth	H (cm)	7.96	7.19	9.61
Roughness high	k (mm)	10	10	10
Mean flow velocity	U_m (cm/s)	12.56	13.91	10.41
Friction flow velocity	U_* (cm/s)	3.95	3.75	4.34
Maximum flow velocity	U_0 (cm/s)	16.24	19.45	19.18
Channel slope	I_0	1/500	1/500	1/500
Froude number	$U_m/(gH)^{1/2}$	0.14	0.17	0.11
Reynolds number	$U_mH/\square$	10000	-	-

3. Results and discussions

3.1 Effects of sediment concentration on-resistance characteristics

Figure 3 and figure 4 show the effects of sediment concentration (Cv) and the PSA solution concentration (Cw) on the normal depth of surface roughness in the two-dimensional ribs. The vertical axis represents the difference in normal depth between the sediment-laden flow, PSA solution, and the clear water flow, which has been non-dimensionalized by the following equation:

$$\Delta h / ho \ (Ci = 0) = \{ho \ (Ci\ ) - ho \ (Ci = 0)\} / ho \ (Ci = 0) \tag{1}$$

In the sediment-laden flows, C_i=C_V; in the PSA solution flows, C_i=C_w. Regardless of the levels of roughness height [k=5 mm (λ/k=8) or k=10 mm (λ/k=10)], both normal depth and resistance were small when the levels of the sediment volumetric concentration were less than 8.5% (C_v<8.5%) as shown in figure 3. By contrast, both normal depth and resistance were large when all experimental parameters were the same except the levels of sediment volumetric concentration exceeded 8.5% (C_v>8.5%).

When the roughness height was k=5 mm, the minimum value was recorded at C_v=4–6%. A significant difference [$\Delta h / h_0 (C_V = 0) = -0.15$] was identified at C_v=6% when the roughness height was k=10 mm. At volumetric sediment concentration C_v=10%, when k=5 mm, $\Delta h / h_0 (C_V = 0) = 0.19$, and when k=10 mm, $\Delta h / h_0 (C_V = 0) = 0.15$, thus indicating a marked increase in the depth.

In the aftermath of the Tondano River flood disaster in Manado, the volumetric concentration of the sediment was about 9.8%. Consequently, the river channel plan specified the levels of basic flood discharge, which represented 9.8% sediment discharge in addition to the amount of water. In the hyper-concentrated sediment-laden flows that contain large sediment, the rate of flow and the resistance drastically increased. The effect of PSA solution concentration (C_w) on the normal depth under the roughness heights of k=5 mm

(λ/k=8) and k=10 mm (λ/k=10) showed a similar trend as that for the effect of kaolin sediment concentration (C_v) as shown in figure 4. Compared to the clear water flow, the normal depth was small at concentration levels C_w<600, but tended to be larger at concentration levels from C_w>600 mg/l. A PSA solution concentration C_w>600 mg/l corresponded to C_v=8.5% in kaolin sediment concentration. The minimum value was recorded $\Delta h/h_0 (C_W = 0) = -0.10$ where roughness height k=5 mm and $\Delta h/h_0 (C_W = 0) = -0.11$ at k=10 mm in the PSA C_w=300 mg/l solution. A similar tendency as that for the kaolin sediment concentration was observed. The PSA solution concentration C_w=300 mg/l corresponded to C_v=6% in kaolin sediment concentration.
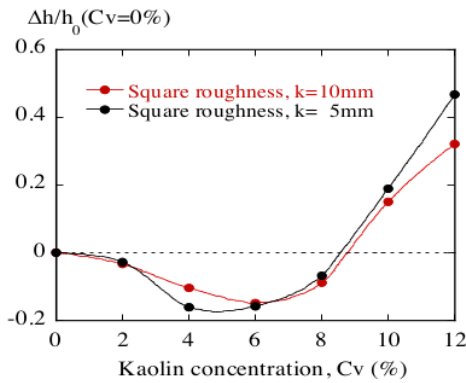

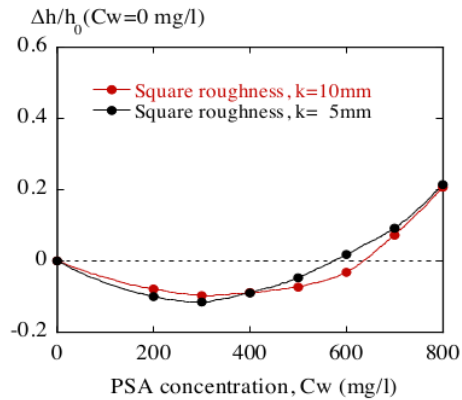**Figure 3.** Effects of hyper-concentrated sediment on resistance.

Figure 4. Effects of PSA solution on resistance.

3.2 Total resistance coefficient and concentration
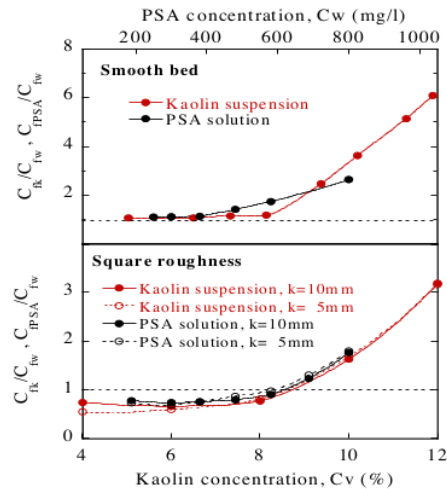

Figure 5. Relationship between total resistance coefficient and concentration.

The vertical axis in figure 5 shows the relationship between the ratio of the total resistance coefficient of kaolin suspension to the total resistance coefficient of clear water (c_{fK}/c_{fW}) and the ratio of the total resistance coefficient of PSA solution to the total resistance coefficient of clear water (c_{fPSA}/c_{fW}).

The resistance coefficient c_{fK}/c_{fW} changes in the kaolin suspension when Cv= 2-8 %, giving a coefficient of 0.54-0.98 for roughness height of k=5 mm, and a coefficient of 0.66-0.91 for roughness height of k=10 mm. Therefore, the resistance coefficients of sediment-laden flows are smaller than that of clear water flow. The minimum value for the resistance coefficient was 0.54, obtained in the Cv=4% case, in which the roughness height was at k=5 mm. However, the minimum value for the resistance coefficient was 0.66 at k=10 mm, in the Cv=6% case.

The total resistance coefficient (c_{fPSA}/c_{fW}) in the PSA solution with concentration levels of Cw=200-600 mg/l ranged between 0.73-1.0 at roughness height k=5 mm and 0.74-0.91 at roughness height k=10 mm. This showed a similar trend as that observed for sediment-laden flows. The resistance coefficient c_{fK}/c_{fW} was approximately 1 in kaolin flow with concentration levels of Cv<8% in the smooth open channel. No significant difference was observed between kaolin sediment-laden flow and clear water flow. The resistance coefficient tended to increase proportionately to the levels of sediment concentration when Cv>8%. It had been suggested that sediment largely diminished form resistance in two-dimensional square ribs. The resistance coefficient (c_{fK}/c_{fW}) for the volumetric sediment concentration Cv=10% case was 1.68 at k=5 mm, 1.63 at k=10 mm, and 3.63 in the smooth open channel. These results indicate a marked increase in resistance. The total resistance coefficients in the PSA solution Cw=800 mg/l, which corresponded to volumetric sediment concentration of Cv=10%, were 1.79 at k=5 mm, 1.76 at k=10 mm, and 2.65 in the smooth open channel. Although these results show similar trends as those of the clear water flow with two-dimensional square ribs, the value of the total resistance coefficients is small in the smooth surface.

The visual observation of the roughness cavity in the side bank of the flume suggests a reason why the resistance coefficient decreased in the sediment-laden flow compared to the PSA solution. This might be attributed to the sedimentation of kaolin that occurred behind the roughness cavity. However, it was impossible to conduct visual observations near the base in the smooth open channel.

3.3 Mean flow velocity and turbulence characteristics
The flow resistance experiment with two-dimensional ribs roughness demonstrated relatively small resistance in the sediment-laden flows with the volumetric sediment concentration Cv<8.5%, whereas the resistance was large at Cv>8.5%, at both roughness heights of k=5 mm (λ/k=8) and k=10 mm (λ/k=10). In this section, the effect of sediment on flow is examined using the flow measurements obtained in the experiment with k=10 mm (λ/k=10) as shown in table 2.

It is extremely challenging to measure the velocity in hyper-concentrated sediment-laden flows. Therefore, PSA solution, which has similar viscosity characteristics as sediment-laden flows, is used as simulant fluid. Flow velocities were measured in detail at the point where the resistance coefficient reached a minimum of 300mg/l and a maximum of 800 mg/l in a weight concentration of PSA solution.

Figure 7 and figure 8 show a color contour plot of time-mean flow velocity in the PSA solution Cw=300 mg/l (corresponding to Cv=6% in kaolin suspension concentration) and the PSA solution Cw=800 mg/l (corresponding to Cv=10% in kaolin suspension concentration). The solid lines in the contour plot represent isolines of the stream function Ψ.

As shown in figure 6, for clear water flow, the streamline that separated from the top of the roughness cavity reattached to the roughness cavity of the bed surface at x/k=4.5, and circulation flow was identified below the separation line. The location of the reattachment point was near the general location of a dune. Isolines of the main flow velocity were projected downward inside the roughness cavity, whereas they were projected upward in the upper layer of the roughness cavity. The separation of the streamline was not identified in either Cw=300 mg/l or Cw=800 mg/l PSA solutions as shown

in figure 7 and figure 8 even inside the roughness cavity, the streamline was almost approximately parallel to the bed surface compared to that in the clear water flow.
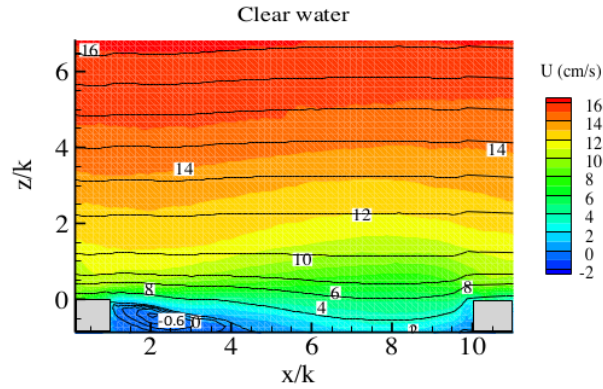

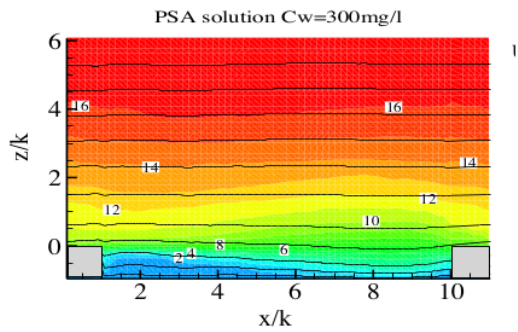**Figure 6.** Colour contours of main flow velocity (clear water).

Figure 7. Colour contours of main flow velocity (PSA solution *Cw*=300mg/l).
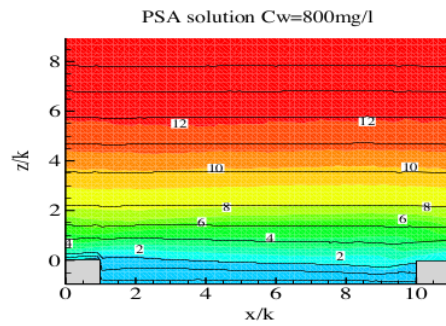
Figure 8. Colour contours of main flow velocity (PSA solution *Cw*=800mg/l).
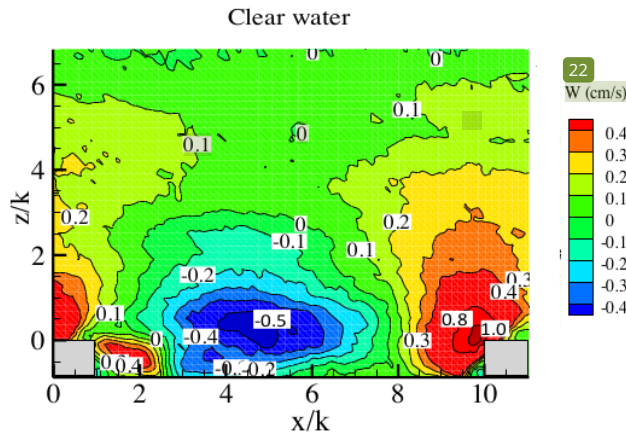

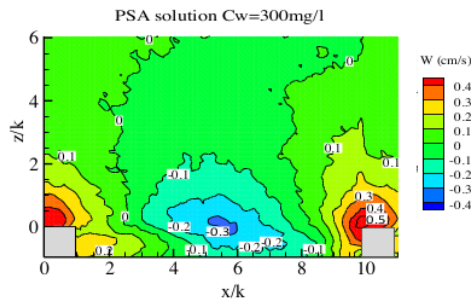**Figure 9.** Colour contour of vertical velocity (clear water).

Figure 10. Colour contour of vertical velocity (PSA solution Cw=300mg/l).

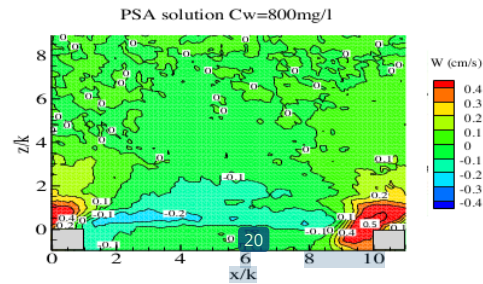**Figure 11.** Colour contour of vertical velocity (PSA solution Cw=800mg/l).

Isolines of the main flow velocity in the PSA solution Cw=300 mg/l show similar patterns as those for clear water. The isoline patterns in the PSA solution Cw=800 mg/l were entirely different; no clear change in the flow direction was detected. A minimal change in the vertical direction was found in the main flow velocity near the surface for both PSA solutions, although this tendency was stronger for the PSA solution Cw=300 mg/l.

Figures 10 and figure 11 show a color contour plot of time-averaged flow for the vertical velocity for both PSA solutions [Cw=300 mg/l (corresponding to Cv=6% in kaolin sediment concentration), and Cw=800 mg/l (corresponding to Cv=10% in kaolin sediment concentration)]. The vertical flow velocity W caused a strong upward current upstream of the roughness cavity, a weak upward current downstream of the roughness cavity, and a downward current in the wide-area near the center of the roughness cavity. The upward and downward currents were small enough to be negligible in the upper half of the water depth. Compared to the clear water flow as shown in figure 9, the sizes of both upward and downward currents diminished to half in both PSA solutions. The momentum transport at the boundary surface was small and negligible, especially for the PSA solution Cw=800 mg/l.

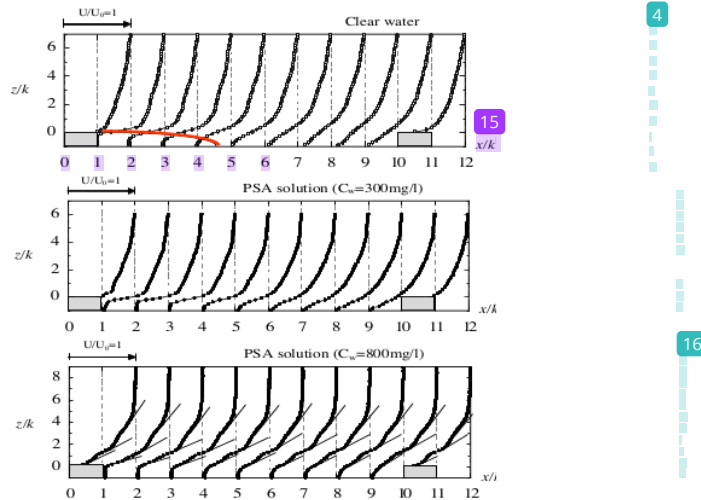*3.4 Vertical distribution of main flow velocity*

Figure 12. Vertical distribution of main flow velocity, U.

Figure 12 presents how the vertical distribution of the main flow velocity changes in clear water and both of the PSA solutions (C_w=300 mg/l and C_w=800 mg/l). The vertical and horizontal axes were non-dimensionalized by the roughness height k. The velocity scale was non-dimensionalized by the maximum flow velocity U_0 near the free surface. The vertical axis was shifted in the flow direction by the unit of x/k=1.0. There were three locations where the rate of change for the main flow velocity in the vertical direction reached maximum values for the PSA solution C_w=800 mg/l, which are indicated by the solid line. The vertical distribution of the main flow velocity showed characteristics of a free-mixing layer behind the roughness cavity, which suggested the growth of an internal boundary layer along the bed surface further downstream and the influence of flow acceleration due to the forward pressure gradient. Unlike that in the clear water flow, the high-shear velocity field was clearly identified at the three locations for both PSA solutions, especially for the PSA solution C_w=800 mg/l. The solid line in the clear water control indicated the flow separation line. Flow separation and the resultant development of circulation flows were not pronounced for the PSA solutions. These results indicate that the influence of circulation flows is smaller in high-viscosity PSA solutions than in clear water, so that form resistance becomes smaller in relative terms.
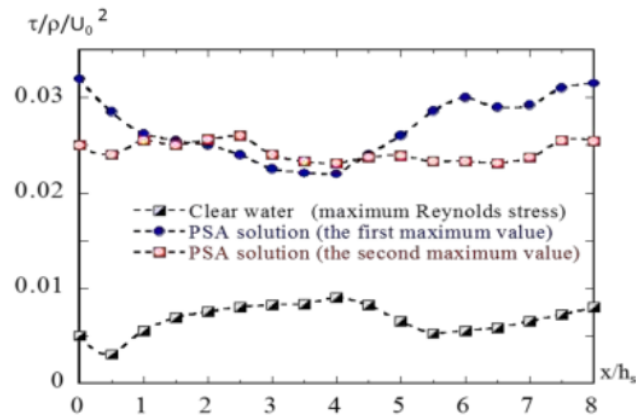
3.5 Streamwise distribution of total shear stress

Figure 13. Streamwise distribution of total shear stress.

Figure 13 shows the change in the maximum value of shear stress in the flow direction. The maximum value of shear stress is smaller in the PSA 300mg/l case than in the clear water case except for the value recorded in the upstream of the roughness cavity. In the PSA solution 800mg/l case, the first maximum value of shear stress tended to decrease from the downstream of the roughness and continuously decrease in the wide area of the roughness cavity. The second maximum value does show notable change throughout the roughness cavity region. Under the experimental conditions, the maximum value for shear stress in the PSA solution was approximately 4.2-10 times the shear stress value in clear water flow. The reasons why the total resistance coefficient decreased up to 26% relative to the clear water case in the PSA solution 300 mg/l case (6% sediment concentration) with the increase in the concentration of the PSA solution, a non-Newtonian fluid, might be attributed to: (1) the increase in the concentration associated with the viscosity was reduced in the flow direction by the turbulence caused by flow separation from the roughness element and (2) the decrease in momentum transport and energy losses due to turbulence. The total resistance coefficient tended to increase again in the solution with the concentration level higher than the PSA solution 300mg/l.

4. Conclusion and recommendation

Compared to clear water flow, resistance is small in sediment-laden flows with volumetric sediment concentrations of $Cv<8.5\%$, whereas resistance is large with volumetric sediment concentrations of $Cv>8.5\%$, at both $k=5$ mm ($\lambda/k=8$) and $k=10$ mm ($\lambda/k=10$) roughness heights.

No prominent separate circulation flow is observed in the color contour plot of time-mean flow for the main flow velocity in both PSA solutions $Cw=300$ mg/l (corresponding to $Cv=6\%$ in kaolin sediment concentration), and $Cw=800$ mg/l (corresponding to $Cv=10\%$ in kaolin sediment concentration)]. This result suggests that the form resistance in high-viscosity PSA solutions is smaller than that observed in clear water.

The spatial distribution of viscous stress in the PSA solution showed a tendency similar to the tendencies of the spatial distributions of turbulence intensity in the streamwise direction and the shear rate. Concerning streamwise distribution of the maximum shear stress, in case of PSA solution 800 mg/l, the first maximum value of shear stress tended to decrease from the downstream of the roughness and continuously decrease in the wide area of the roughness cavity, while the second maximum value does show notable change throughout the roughness cavity region. The maximum value for shear stress in the PSA solution 800 mg/l was approximately 4.2 - 10 times the shear stress value in clear water flow.

The primary reason why the total resistance coefficient for highly viscous PSA solution 800 mg/l (10% sediment concentration) increased about 176% of the clear water case might be attributed to the increase in the viscous resistance caused by the shear-thinning effect of non-Newtonian fluids.

Need more adequate equipment and precise measurement systems to obtain more accurate experimental results for further study.

References

[1] Bradley J B, and Mc Cutcheon S C 1985 The effects of high sediment concentration on transport processes and flow phenomena *Proc. Int. Conference Erosion Debris Prevention* Japan

[2] Ashida K, Yamano K and Kanda M 1985 Study on hyperconcentrated flow (1) *Annuals, Disaster Prevention Research Institute* **28** (2) 367-377

[3] Coussot P 1992 *Rheology of Debris Flow – Study of Concentrated Suspensions* (France: INPG Grenoble)

[4] Yang C T, and X Kong 1996 Energy dissipation rate and sediment transport *Journal of Hydraulic Research* **29** (4) 457-474

[5] Toms B A 1948 Some Observations on the Flow of Linear Polymer Solutions though Straight Tubes at Large Reynolds Numbers *Proc. International Congress On Rheology* (Amsterdam North Holland)

[6] Mukanata M 2002 *Study on the flow drag reduction by additives* (Japan Kumamoto University)

[7] Ohmoto T, Sukarno, and L Hendratta 2013 Effects of regularly arrayed roughness on flow resistance and turbulent flow structure in an open channel with square ribs *Journal of Japan Society of Civil Engineering* **68** (4) 901-906

A Study on-resistance characteristics and turbulent structure properties of hyper□concentrated sediment-laden flow

9   centaur.reading.ac.uk
Internet Source
<1%

10   Guangming Tan, Hongwei Fang, Subhasish Dey, Weiming Wu. "Rui-Jin Zhang's Research on Sediment Transport", Journal of Hydraulic Engineering, 2018
Publication
<1%

11   f1000research.com
Internet Source
<1%

12   Eduardo Guzmán, Irene Abelenda-Núñez, Armando Maestro, Francisco Ortega, Andreas Santamaria, Ramon Gonzalez Rubio. "Particle-laden fluid/fluid interfaces: physico-chemical foundations", Journal of Physics: Condensed Matter, 2021
Publication
<1%

13   Feifei Zhang Leighton, Alistair G. L. Borthwick, Paul H. Taylor. "1-D numerical modelling of shallow flows with variable horizontal density", International Journal for Numerical Methods in Fluids, 2009
Publication
<1%

14   Victor Birman. "Chapter 2 Static Problems in Isotropic Rectangular Plates", Springer Science and Business Media LLC, 2010
Publication
<1%

www.sm.luth.se

15   Internet Source   <1 %

16   19january2021snapshot.epa.gov
Internet Source   <1 %

17   L Bodri, B. Bodri. "Flow, stress and temperature in island arc areas", Geophysical & Astrophysical Fluid Dynamics, 2006
Publication   <1 %

18   Soumen Maji, Debasish Pal, Prashanth R. Hanmaiahgari, Umesh P. Gupta. "Hydrodynamics and turbulence in emergent and sparsely vegetated open channel flow", Environmental Fluid Mechanics, 2017
Publication   <1 %

19   Manotosh Kumbhakar, Jitraj Saha, Koeli Ghoshal, Jitendra Kumar, Vijay P. Singh. "Vertical Sediment Concentration Distribution in High-Concentrated Flows: An Analytical Solution Using Homotopy Analysis Method", Communications in Theoretical Physics, 2018
Publication   <1 %

20   escholarship.org
Internet Source   <1 %

21   iwaponline.com
Internet Source   <1 %

22   www.eposters.net
Internet Source   <1 %

23 M. Oettel, S. Dietrich. "Colloidal Interactions at Fluid Interfaces", Langmuir, 2008
    Publication

    <1 %

24 D.L. Kleinman. "Optimization of detection networks. I. Tandem structures", 1990 IEEE International Conference on Systems Man and Cybernetics Conference Proceedings, 1990
    Publication

    <1 %

25 Watanabe, Takahiro, Kohei Tanaka, Masaaki Motozawa, and Yasuo Kawaguchi. "Simultaneous PIV and PLIF Measurement on the Drag Reducing Channel Flow of the Homogeneous Surfactant Solution", ASME/JSME 2011 8th Thermal Engineering Joint Conference, 2011.
    Publication

    <1 %

| Exclude quotes | Off | Exclude matches | Off |
| Exclude bibliography | Off | | |